Resonant Tunnelling Diode Terahertz Sources with up to 1 mW Output Power in the J-Band

Abdullah Al-Khalidi, Khalid Hamed Alharbi, Jue Wang, Razvan Morariu, Liquan Wang, Ata Khalid, José Figueiredo, and Edward Wasige, *Member, IEEE*

***Abstract*— Terahertz (THz) oscillators based on resonant tunneling diodes (RTDs) have relatively low output power, tens to hundreds of microwatts. The conventional designs employ sub-micron sized RTDs to reduce the device self-capacitance and, as a result, realise higher oscillation frequencies. However, reducing the RTD device size leads to lower output power. In this paper we present RTD oscillators which can employ one or two RTD devices of relatively large size, 9 - 25 μm^2, for high power and, at the same time, can oscillate at THz frequencies. This is achieved through low resonating inductances realized by microstrip or coplanar waveguide (CPW) transmission line short stubs with low characteristic impedances (Z_0), which have lower inductance values per unit length and so compensate the increase of the self-capacitance of large area RTD devices. Thus, fabrication using only photolithography is possible. It is also shown that device sizing, which is limited only by bias stability considerations, does not limit device bandwidth. Further, we report a new way to estimate the RTD oscillator output power with frequency. A series of oscillators with oscillation frequencies in the 245 – 309 GHz range and output powers from 0.1 – 1 mW have been demonstrated showing the feasibility of the proposed approach.**

***Index Terms*—Resonant tunnelling diode (RTD), terahertz (THz) sources, photolithography.**

I. INTRODUCTION

RESEARCH on the application of terahertz (THz) waves (0.1 - 10 THz) to ultrahigh-speed wireless communications [1], imaging [2] and other applications is on the rise. Various semiconductor electronic devices and integrated circuits have been reported for THz transmitters and receivers [3]-[5]. Among these devices, the resonant tunneling diode (RTD) has exhibited the highest oscillation frequency close to 2 THz [5]. Advantages of RTDs include the facts that they can operate both as an oscillator/transmitter and detector/receiver [6]; they are compact, consume low power, the output power is easily modulated though the bias network, can be designed to be optically controlled and can operate at room temperature. Thus, RTDs are expected to realise compact, very high bandwidth and low-cost THz electrical transceivers, which are similar to diode-based optical transceivers consisting of a laser diode (LD)/light-emitting diode (LED) and a photodiode.

In our recent work, we have reported RTD oscillators with high output powers in the 0.5-1mW range up to 300 GHz [7]-[10]. We have used this technology to demonstrate 15 Gbps wireless links using W-band RTD oscillators [7], and are now developing such links for future wireless data centres [11]. We have also reported millimeter-wave RTD oscillators with very high dc-RF conversion efficiency (>10%), a tenfold improvement on conventional designs (~1%) [12]. RTDs have the potential to underpin emerging new applications requiring short range high capacity wireless links such as virtual gaming, kiosk downloads, wireless memory sticks, etc. Part of the appeal for RTDs is in their simplicity, e.g. a 1 mW J-band source requires only a single RTD device realised using just photolithography [10], whilst transistor technologies such as CMOS require an array of 8 or more active devices, sub-100 nm high resolution lithography and advanced circuit design techniques [13]. Also, RTDs can provide high performance electronic sources beyond 300 GHz, frequencies that cannot generally be easily covered by any transistor technologies today [14].

In this paper, we provide a comprehensive description of the design approach for the J-band oscillators which were first reported in brief conference publications [9], [10]. This includes a discussion of the device design which involves the use of low peak current density epitaxial designs as opposed to conventionally used high peak current density ones, as well as the use of very low characteristic impedance microstrip transmission line stubs to realise resonating inductances in the oscillator circuits. In addition, a new way to estimate the oscillator output power with frequency is described. The paper is organized as follows: in Section II, a discussion on RTD device bandwidth and sizing, and on RTD oscillator output

Manuscript received June 9, 2019; accepted December 08, 2019. This work was supported in part by the Engineering and Physical Sciences Research Council (EPSRC) of the UK, grant number EP/J019747/1, and in part by the European Commission, grant agreements no. 645369 (iBROW project) and no. 761579 (TERAPOD project), as well as the European Regional Development Fund (FEDER), Competitiveness and Internationalization Operational Programme (COMPETE 2020) of the Portugal 2020 framework RETIOT project (POCI-01-0145-FEDER-016432).

A. Al-Khalidi, J. Wang, R. Morariu and E. Wasige are with the High Frequency Electronics (HFE) Group, James Watt School of Engineering, University of Glasgow (email: abdullah.al-khalidi@glasgow.ac.uk, edward.wasige@glasgow.ac.uk)

K. H. Alharbi and Ata Khalid were with the HFE Group, University of Glasgow. K. H. Alharbi is now with the Department of Electrical and Computer Engineering King Abdulaziz University, Jeddah 21589 Saudi Arabia, while Ata Khalid is now with Centre for Electronic Warfare Information and Cyber, Cranfield University, Shrivenham SN68LA, UK

L. Wang is with the Shanghai Electro-Mechanical Engineering Institute, Shanghai 201109, China.

J. Figueiredo is with the Departamento de Física da Faculdade de Ciências da Universidade de Lisboa, Campo Grande, 1749-016 Lisboa, Portugal.

power considerations is provided. Details of the fabrication of RTD devices and their current-voltage (*I-V*) characteristics are also provided. In Section III, the design and fabrication of the J-band RTD oscillators is described. The characterization of the oscillators including a discussion of the experimental results is described Section IV. Conclusions and future work are given at the end of the paper in Section V.

II. RTD Device sizing, Fabrication & Characterisation

A. Device Sizing and Bandwidth Considerations

The InP-based RTD device typically consists of a narrow bandgap material (4 - 6 nm thick $In_{0.53}Ga_{0.47}As$ quantum well) sandwiched between two thin wide bandgap materials (1 - 3 nm AlAs barriers), making up the double barrier quantum well (DBQW) structure. The structure is completed by lightly doped $In_{0.53}Ga_{0.47}As$ spacer layers, n-type emitter/collector layers and highly doped $In_{0.53}Ga_{0.47}As$ contact layers on either side of the DBQW. The high frequency and RF output power capability of an RTD device can be estimated from this epi-structure and the device *I-V* characteristic, which exhibits a negative differential resistance (NDR) region where the current drops with increasing bias and which bestows the RTD with its unique characteristics for high frequency oscillator realisation. The cut-off frequency f_{max} is given by [15]

$$f_{max} = \frac{G_n}{2\pi C_n}\sqrt{\frac{1}{R_S G_n} - 1} \tag{1}$$

where C_n is the RTD self-capacitance, G_n is the absolute value of maximum negative differential conductance, and R_S is the contact resistance. Here, $C_n = \frac{\epsilon_0 \epsilon_r A}{d}$ is the device geometrical capacitance (which is augmented with the quantum-well capacitance, C_{qw}) with ε_r the relative permittivity of InGaAs, ε_o is the permittivity of free space, *A* is the area of the device, and *d* is the thickness of the DBQW structure including the spacer layer on the collector side; $G_n = \frac{3}{2}\frac{\Delta I}{\Delta V} = \frac{3\Delta J A}{2\Delta V}$ and $R_S = \frac{\rho_c}{A}$, with ρ_c being the specific contact resistance; ΔI and ΔV are the peak-to-valley current and voltage differences, respectively, and are found from the measured *I-V* characteristics; and $\Delta J = \Delta I/A$ is the peak to valley current density. Therefore (1) can be re-written as

$$f_{max} = \frac{d}{2\pi\epsilon_0\epsilon_r}\frac{2\Delta J}{3\Delta V}\sqrt{\frac{2\Delta V}{3\Delta J\rho_c} - 1} \tag{2}$$

For a given RTD device, it can be deduced from (2) that the cut-off frequency is independent of device sizing and is only related to ΔJ and ρ_c which are mostly determined by the layer design and the fabrication process, respectively. The RF output power of an RTD oscillator, on the other hand, is given by $(3/16)\Delta V\Delta I$ [16], and therefore requires designs which maximize ΔV and ΔI. Thus, RTD epi-designs which provide a large ΔV (which is largely independent of device size) and the largest possible RTD devices (for large ΔI) are desirable since there are no bandwidth limitations associated with device sizing.

Conventionally, however, the commonly used figure-of-merit for RTDs is the peak current density (J_P), the current at which the device starts to exhibit NDR. State of the art RTD oscillators employ epitaxial structures with J_P of around 700 kA/cm^2 which unfortunately exhibit low peak-to-valley voltage difference ΔV of ~0.2V, poor peak to valley current ratio (PVCR) of ~1.2, leading to low (μW) output power and poor efficiency, e.g. [17]. Also, such high J_P structures ($J_P > 6$ mA/μm^2) necessarily require small sub-micron RTD devices sizes which require ultra-low contact resistances, suffer thermal issues and have limited available power capability [17]. Through careful device engineering, this approach has nonetheless provided state-of-the-art performance [18]. Therefore, in contrast to the conventional approach which aims to use the smallest devices through high ΔJ epi-designs, we propose to employ epitaxial designs with low self-capacitance and low ΔJ since the total device current can be adjusted through device sizing. Now considering the fact that the existence of the NDR means that RTD devices are prone to oscillations when biased in this region, a shunt resistance R_E is usually connected across the device so as to eliminate these bias oscillations. It must satisfy $R_E > \frac{1}{G_n}$ which for a given R_E establishes the maximum device size, A_{max}, as [19]

$$A_{max} R_E < \frac{2\Delta V}{3\Delta J} \tag{3}$$

R_E is usually chosen to be in the 10-20 Ω range. From (3), it is clear that the use of RTD design with large ΔV and moderate ΔJ is key to realizing large devices which can provide high power at THz frequencies. In this paper, we employ epi-structures with moderate current density of 3mA/um^2 with large ΔV of 0.6V, good PVCR of 3 and good (mW) output power. To achieve this, the RTD and load (G_L) impedance must also be matched, i.e. $G_n = 2G_L$, as will be described in Section 2C.

B. Device Fabrication and Characterisation

The layer structure of the RTD wafer that was used in the oscillators reported here is shown in Figure 1a. It was grown by molecular beam epitaxy (MBE) by IQE Ltd on a semi-insulating InP substrate. It employs a 4.5 nm indium gallium arsenide ($In_{0.53}Ga_{0.47}As$) quantum well, 1.4 nm aluminium arsenide (AlAs) barriers and 25 nm lightly doped $In_{0.53}Ga_{0.47}As$ spacer layers. The collector and emitter layers are made of highly doped $In_{0.53}Ga_{0.47}As$ material doped with Si.

The RTD devices were fabricated using optical lithography. Chemical wet etching (H_3PO_4:H_2O_2:H_2O = 1:1:38) was used to define the RTD mesa. Polyimide from HD MicroSystems was used for device passivation. The measured *I-V* characteristic of a 4 μm × 4 μm RTD is shown in Figure 1b and a micrograph of a fabricated device is shown in Figure 1c. The device exhibits a peak-valley bias voltage difference (ΔV) of around 0.7 V and peak-valley current difference (ΔI) of around 25 mA. The 5 μm × 5 μm RTD had the same ΔV of 0.7 V but a larger ΔI of 39 mA.

From S-parameter measurements, the small signal equivalent circuit for the RTD was extracted using direct optimisation. Figure 2a shows the used small signal equivalent circuit, while Figure 2b shows the fit between the modelled and measured Z-parameters. For the 4 μm × 4 μm RTD extracted device capacitance was around 2.8 fF/μm^2 in the positive differential resistance (PDR) regions, and estimated to be around 3.75 fF/μm^2 in the NDR as described in [20]. It comprises the geometrical capacitance (computed from device geometry) and quantum capacitance ($C_Q = -G_n/v_C$), where v_C is the electron escape rate from the quantum well to the collector. This self-capacitance is low enough to allow the realization of millimeter-wave or THz oscillators. The extracted contact resistance was 2.8 Ω and $G_n = 54$ mS in the NDR giving f_{max} of around 350 GHz for the 4 μm × 4 μm devices.

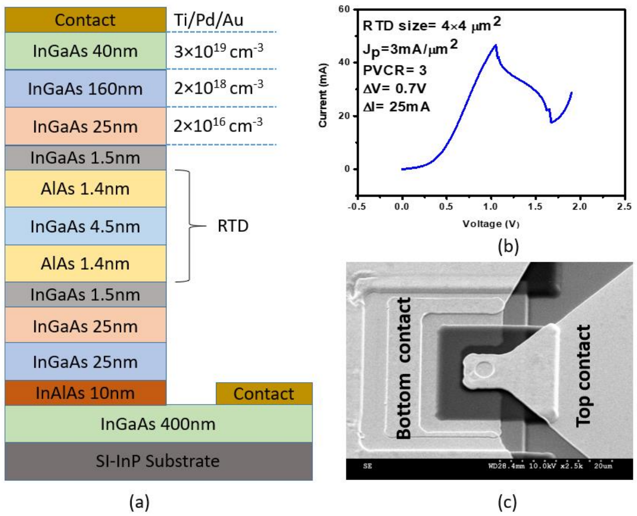

Figure 1: (a) Epitaxial RTD layer structure, (b), Measured *I-V* characteristics of the 4 μm × 4 μm RTD device, (c) Scanning electron microscope (SEM) micrograph of the fabricated RTD device.

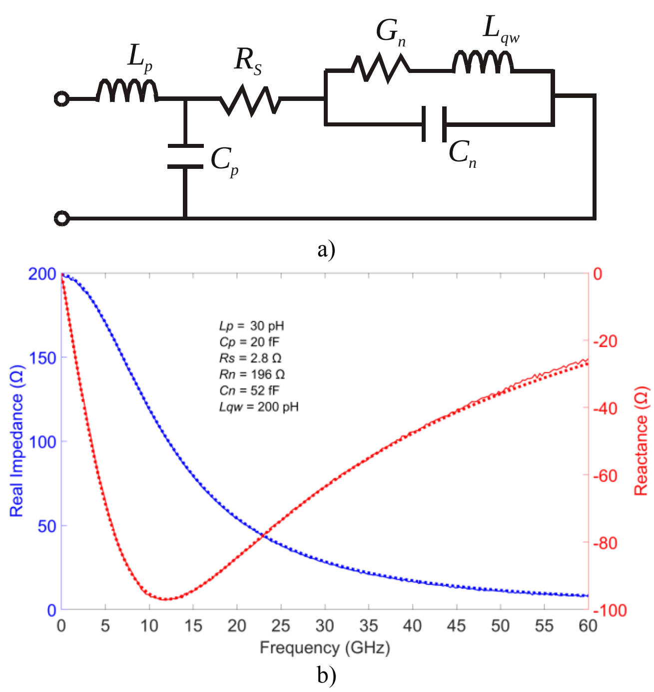

Figure 2: a) Small-signal equivalent circuit of an RTD. R_S is the contact and access resistance, G_n the device conductance, C_n the device self-capacitance and L_{qw} the quantum-well inductance. L_p and C_p model the bond pad inductance and capacitance. b) Modelled (dotted lines) and measured (solid lines) Z-parameters (input impedance) up to 60 GHz of the 4 μm × 4 μm RTD in the PDR region ($V_{bias} = 0.2$ V).

C. *Oscillator Circuit, Output Power & Oscillation Frequency*

The typical RTD oscillator circuit is shown in Figure 3(a), with the corresponding RF equivalent circuit shown in Figure 3(b), in which the RTD is modeled by its *I-V* characteristic in parallel with the self-capacitance. The device contact resistance is neglected in this description. The resistor R_B and inductor L_B denote the bias cable resistance and inductance, respectively, while R_E is the bias stabilization resistor. The capacitor C_E provides a short-circuit path for the RF signal to ground, and so no RF power is dissipated over R_E. This capacitor also provides a short-circuit termination for the transmission line used to realise inductance L which is designed to resonate with the RTD self-capacitance C_n. Here, the relation $\omega_0 L = Z_0 tan\beta l$ is used, where ω_0 is the oscillation frequency, β the phase constant and l the length of the stub. The resistance R_L represents the load, 50 Ω in our case, which is provided by the spectrum analyser or power meter during measurement. Capacitor C_{Block} prevents any dc from reaching the measurement equipment.

For this oscillator circuit, it can be shown that the power delivered to the load $G_L = 1/R_L$, i.e. the power generated by the diode, is given by [16]

$$P_L' = \frac{2(G_n - G_L)G_L}{3b} \tag{4}$$

with $b = \frac{2\Delta I}{3\Delta V^3}$. The theoretical maximum generated power (P_{max}) occurs when $G_L = G_n/2$ and (4) reduces to the commonly used expression:

$$P_{max} = \frac{3}{16}\Delta V \Delta I \tag{5}$$

The derivation of (4), however, assumes an ideal NDR device and so the effect of parasitic elements is not included. The variation of oscillator output power with frequency is therefore usually estimated using either of the two empirical expressions: $P_{max} \approx \frac{3}{16}\Delta V\Delta I \cos(\tau_{RTD})$ [20] or $P_{max} \approx \frac{3}{16}\Delta V\Delta I\left(1 - \frac{f^2}{f_{max}^2}\right)$ [22], with τ_{RTD} being the carrier transit time through the device, and f the oscillation frequency.

In this paper, we present an analytical method for determining the variation of the RTD oscillator output power with frequency which accounts for the contact resistance R_S of the RTD [19]. Figure 4(a) shows the RF equivalent circuit of an RTD oscillator, including the contact resistance. It is redrawn in Figure 4(b), in which the passive elements are lumped together, and redrawn again in Figure 4(c) as a parallel resonant circuit. Here, the passive elements including the contact resistance of the RTD are replaced by an equivalent admittance, $G_L' + jB$ [19], with G_L' being the equivalent load conductance and B the equivalent susceptance. Using basic circuit analysis, G_L' and B can be expressed as:

$$G_L' = \frac{R_S + \frac{k}{1+kG_L}}{\left(R_S + \frac{k}{1+kG_L}\right)^2 + \left(\frac{\omega L}{1+kG_L}\right)^2} \tag{6}$$

$$B = \frac{\frac{\omega L}{1+kG_L}}{\left(R_S+\frac{k}{1+kG_L}\right)^2+\left(\frac{\omega L}{1+kG_L}\right)^2} \tag{7}$$

where $k = \omega^2 L^2 G_L$ with $G_L = 1/R_L$.

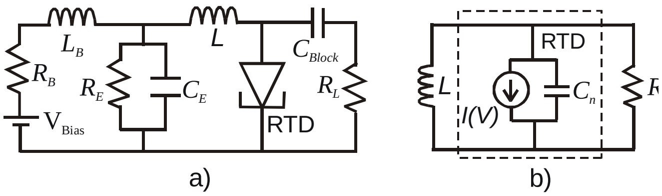

Figure 3: a) Typical single RTD oscillator schematic circuit diagram, b) RF equivalent circuit diagram of RTD oscillator, with the RTD modelled as voltage controlled current source and its self-capacitance, but with its contact resistance neglected.

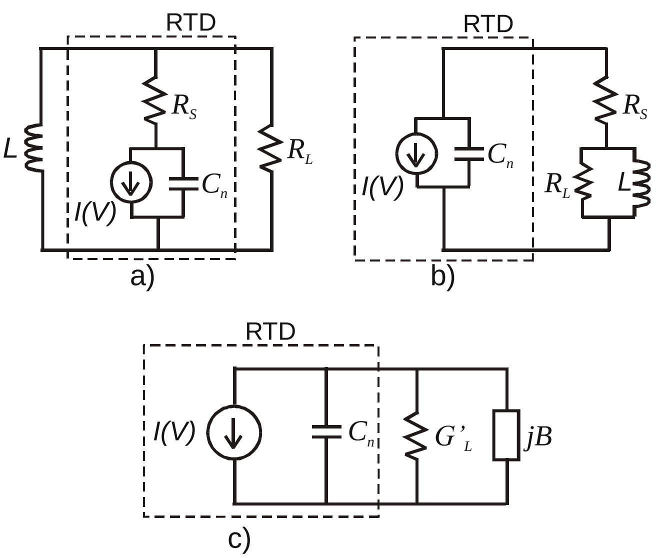

Figure 4: a) RF equivalent circuit of an RTD oscillator including the contact resistance, b) circuit redrawn with the RTD contact resistance and extrinsic passive elements grouped together, c) circuit redrawn further as a parallel resonant circuit.

The resonant frequency ω_0 of the circuit in Figure 4(c) can be determined from $\omega_0 C_n = B$ and (7) to be

$$\omega_0 = \frac{\sqrt{(L - C_n R_S^2)}}{LC_n(1+R_S G_L)} \tag{8}$$

From (8), it is clear that

$$L > C_n R_S^2 \tag{9}$$

if the resonant frequency is to be real. This means that if L is chosen to be less than $C_n R_S^2$ then the circuit becomes stable. It is worth to note that (9) was previously derived in [15] using only circuit stability considerations, which is an indirect validation of this analysis.

Since the circuits of Figures 3(b) and 4(c) are identical, the power delivered to the equivalent load G_L' is given by re-writing (4) as

$$P_L' = \frac{2(G_n - G_L')G_L'}{3b} \tag{10}$$

and, so that the power delivered to the actual load resistance R_L is given by

$$P_L = \frac{R_L''}{R_S + R_L''} \frac{2(G_n - G_L')G_L'}{3b} \tag{11}$$

where

$$R_L'' = \frac{\omega^2 L^2 G_L}{1+\omega^2 L^2 G_L^2} \tag{12}$$

Note that the apparent load G_L' changes with frequency and so does not present an ideal load for maximum output power, i.e. output power drops with increasing frequency. At any given frequency, an optimum value of the oscillator load G_L may be found. For the simplified RTD equivalent circuit with only one parasitic component (R_S), the maximum output power predicted by (11) can be considered as an upper limit.

Using (11), the calculated/expected output power as a function of frequency for a single 4 μm × 4 μm RTD device oscillator is shown in Figure 5 (solid trace). Here, the device parameters ΔV = 0.7 V and ΔI = 25 mA and R_S = 2.8 Ω have been used. As seen in Fig.5, the cut-off frequency is around 340 GHz, which is consistent with that found using (1). The expected output power is about 0.5 mW at 300 GHz. Figure 5 (dashed trace) also shows the expected oscillator performance if a lower contact resistance of, say 1.4 Ω, was used – higher output power and higher bandwidth become possible. The expected output power becomes 2.5 mW at 300 GHz. This is feasible since the measured specific contact resistance using a standard recipe for the devices reported here is $\rho_C = 50$ Ω-μm^2 [23], and this can be reduced significantly using the approach in [24] or similar. Work in this regard is already underway.

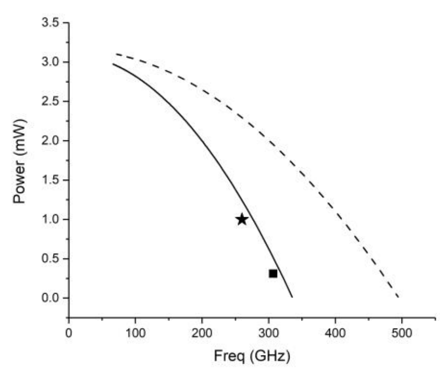

Figure 5: Variation of output power with oscillation frequency for an RTD oscillator employing a 4 μm × 4 μm device ($C_n = 60$ fF) with a $R_S = 2.8$ Ω (solid line, $f_{max} \approx 340$ GHz & $P_{max} \approx 0.5$ mW at 300 GHz; while for $R_S = 1.4$ Ω (dashed line, $f_{max} \approx 500$ GHz & $P_{max} \approx 2.5$ mW at 300 GHz). Measured output powers at 260 GHz and 307 GHz (see Section IV) are also shown.

III. Oscillator Design and Fabrication

Two oscillator topologies were implemented, one employing a single RTD device (Figure 3(a)) and the other two RTD devices. The double RTD oscillator topology is fully described in [8], [9]. The single RTD oscillator employed a microstrip short stub resonator, while the double RTD oscillator a CPW short stub. The oscillation frequency was estimated through the choice of an inductance which would resonate with the extracted small signal device capacitance. Without validated large signal RTD models, non-linear oscillator simulations were not possible, and so a series of oscillators with varying lengths of transmission line stubs were fabricated to experimentally evaluate the performance. The area of each oscillator was about 400 μm × 300 μm, and so a 2 cm^2 sample has over 100 oscillators.

For the double RTD oscillator, the inductance L was realised by appropriate lengths of CPW transmission lines on a semi-insulating InP substrate with Z_0 of 25 Ω, 32 Ω, and 50 Ω shorted by the bypass capacitor C_E. The signal lines widths were 126 μm, 110 μm, and 60 μm and the gap distances between the signal lines to the ground planes were 7 μm, 15 μm, and 40 μm, respectively. For the microstrip RTD oscillators, the resonating inductance was realized by a shorted microstrip transmission line. The microstrip line consisted of a 20 µm wide signal line on top of a 1.2 μm thick polyimide of dielectric constant 3.5, which is spun and cured on a metal (Au) ground plane on the InP substrate. With this configuration, the characteristic impedance of the microstrip line is 10.4 Ω. The CPW and microstrip transmission line dimensions were calculated using the ‘Linecalc’ tool in ADS software [25]. For the 300 GHz oscillators, the required length of a shorted microstrip line (with Z_o =10.4 Ω) was 88 μm compared to 3 μm if a CPW stub with Z_o = 50 Ω was employed, which illustrates the fabrication advantage of the microstrip implementation.

The modelling of the passive parts, such as the resonating inductance and MIM capacitors, was done electromagnetic simulations using HFSS software and validation of the models done via S-parameter measurements [23]. Figure 6a shows, for instance, the layout of the microstrip inductor test structure. It comprises an 88 µm long microstrip stub in series with a 70 µm long CPW line on one side (port 1), and a similarly long CPW line on the other side (port 2) of a terminating/decoupling capacitor, C_E. At high frequencies (>30 GHz in this case) when C_E acts as a short-circuit, the combined inductance of the CPW/microstrip stub, and CPW stub can be extracted from S-parameters, respectively, after conversion to Z-parameters. Design/fabrication details of C_E are given the next paragraph. The extracted and simulated inductance of the microstrip short stub is shown in Figure 6b over the 30 GHz to 65 GHz range, and show a good fit between the measured and simulated values. The inductance of the microstrip short stub was also simulated up to 300 GHz and is shown in Figure 6c. Clearly, the inductance increases with frequency and this would impact actual oscillation frequencies of the J-band RTD oscillators.

For the oscillator fabrication, all features were defined by photolithography. The stabilizing resistor R_E was realised from a 33 nm thin film NiCr which has a sheet resistance of 50 Ω/square. The designed resistor value was 22 Ω, realised with dimensions of 300 μm × 130 μm. Metal-insulator-metal (MIM) capacitors were designed and fabricated to realise C_E and the dc-block in the circuit. The dielectric layer used was Si_3N_4 with 75 nm thickness which corresponds to 0.8 fF/μm^2. It was deposited using inductively coupled plasma (ICP) chemical vapor deposition (CVD). The designed value of C_E was 10 pF realised with MIM size of 210 μm × 60 μm) and that of dc-block capacitor was 1.3 pF realised with MIM size of 20 μm × 80 μm. Measurements of process control structures confirmed that the realised structures had expected values within ±10% [23]. A micrograph of one of the microstrip RTD oscillators is shown in Figure 7.

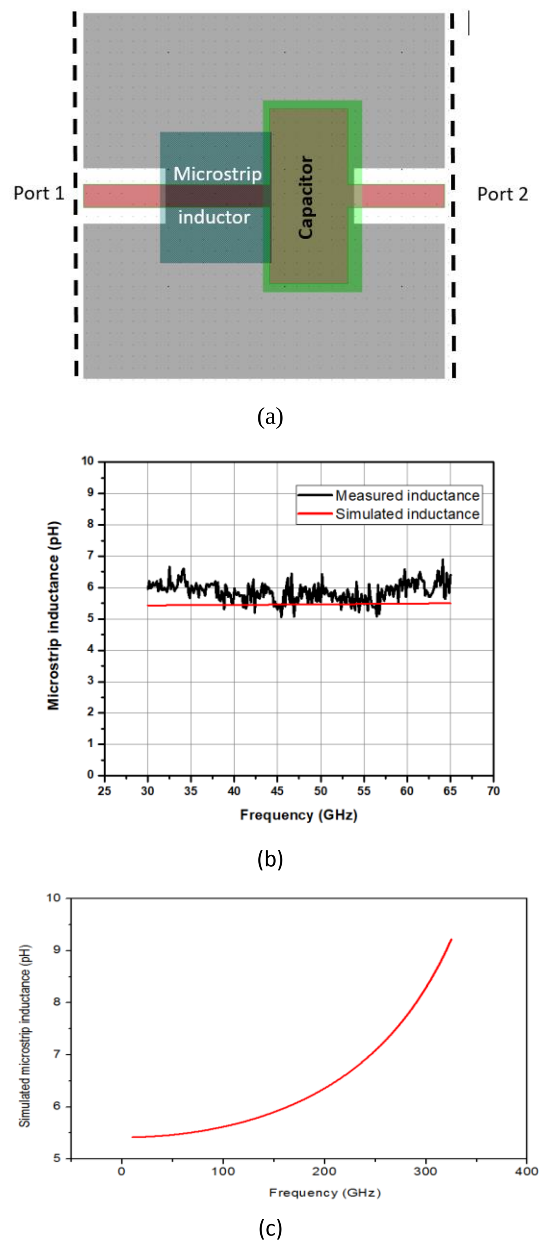

Figure 6: (a) Layout of the microstrip inductor test structure. (b) Measured and simulated inductance of an 88-μm long microstrip stub terminated in a 210 pF capacitor. (c) Simulated inductance of an 88-μm long microstrip short stub up to 300 GHz.

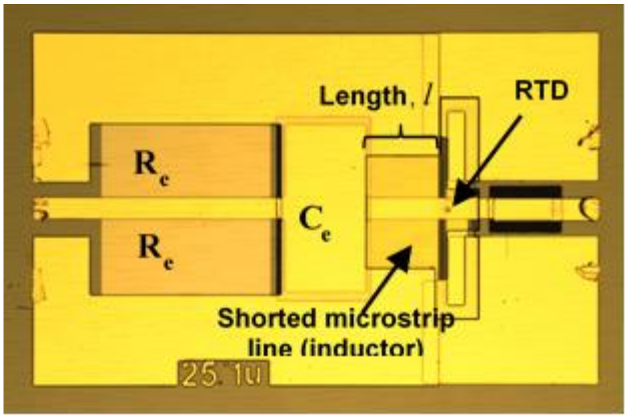

Figure 7: Micrograph of a fabricated J-band microstrip RTD oscillator. Chip size is 400 μm × 300 μm.

IV. Oscillator Characterisation

A. Measurement Setups

The fundamental oscillations of the fabricated oscillators were measured on-wafer using the dc-50 GHz the Keysight E4448A spectrum analyser with appropriate down conversion mixers for higher frequency ranges. The block diagram of the measurement setup is shown in Figure 8(a). The spectrum was characterized from dc through the various bands to confirm the fundamental oscillations. For the J-band (220 – 325 GHz) measurement, the setup consisted of a J-band GSG probe, a J-band harmonic mixer from Farran Technology with a specified conversion loss of approx. 50 dB and a diplexer was used to separate the local oscillator (LO) and intermediate frequencies (IF). The actual output power was measured directly by a calibrated power meter (Erikson PM5). Since the input of power sensor head is WR-10 (W-band) waveguide, a WR-3 to WR-10 tapered waveguide was used as shown in Figure 8(b), and therefore losses due to the probe (3 dB) and waveguide (0.5 dB) were taken into account in determining the actual output power. Figure 8(c) shows a micrograph of one of the fabricated oscillators during on-wafer characterization.

Figure 9(a) shows the measured oscillator spectrum of a 4 μm ×4 μm double RTD oscillator with a 10 µm long 25 Ω CPW shorted stub. The fundamental oscillation was at 307 GHz with 0.31 mW output power. The highest measured and calibrated output power of 1 mW was from a single 4 μm × 4 μm RTD device oscillator at a fundamental frequency of 260 GHz. The measured corrected spectrum is shown in Figure 9(b). The line width was 2MHz at -10dB below the peak power, indicating that the oscillators have relatively low phase noise. The actual measured oscillator power was 0.5 mW before correcting for waveguide taper and probes losses of 3 dB. A picture of this actual measurement is shown in Figure 10. This oscillator exhibited a modulation bandwidth of >100 GHz and has been used in short range multi-gigabit wireless experiments [10].

Table I summarizes the measured and designed oscillation frequencies (in parenthesis) of the different oscillators with different device sizes and different shorted stub designs (lengths and characteristic impedances Z_0). It can be seen that the difference between the designed and measured frequency varies from 3% to 30%. The difference is larger for shorter CPW stubs possibly due to limited resolution with photolithography (alignment accuracy around 1 μm), and so large discrepancies can occur with very short lines. Other reasons include the increased inductance per unit length of the longer microstrip line inductors as noted earlier (Fig. 6c) as well as reduced effective device size due to anisotropic wet etching (100 nm/min), e.g. for a central top contact RTD mesa size of 16 µm^2 the effective device size is estimated to be 12.8 µm^2 for the typical mesa height of 400 nm. Nonetheless, it can also be seen that consistently high output powers of around 0.2 – 1 mW were achieved across various oscillator designs in the 245 – 309 GHz range. The large variation in output power may be attributed to lack of large signal analysis at the design stage, as no impedance matching was accounted for. Nonetheless, the highest measured power is consistent with the analysis given in Section IIC. The dc-RF conversion efficiency is also low, around 0.12% due to the power dissipated by the stabilizing resistor. This is being addressed in future designs which will employ a series resistor-capacitor bias network which draws no dc current [12].

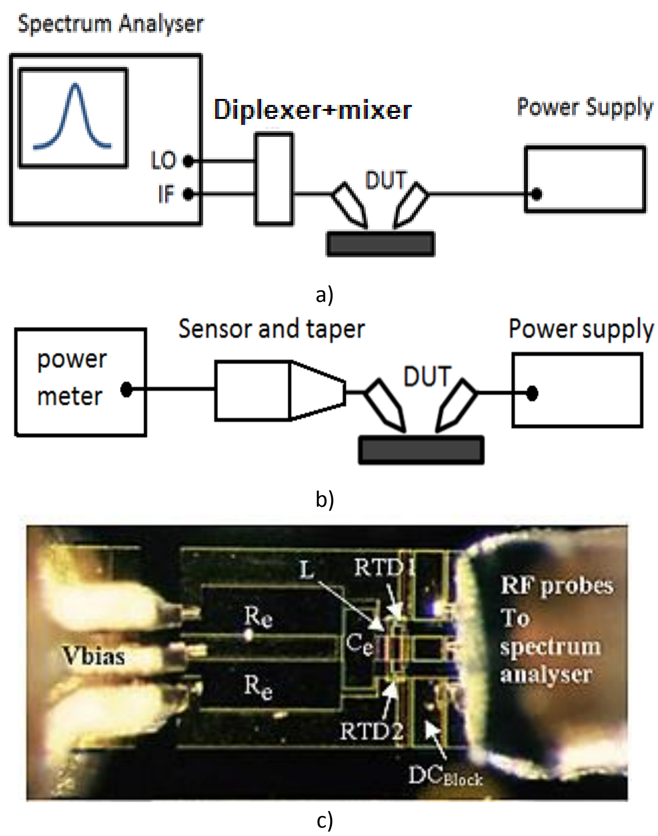

Figure 8: Schematic block diagram showing on-wafer measurements setup: (a) Spectrum measurement, (b) Power measurement, and (c) Micrograph of fabricated oscillator during on-wafer measurement.

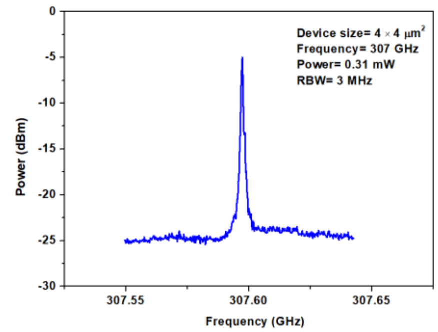

a)

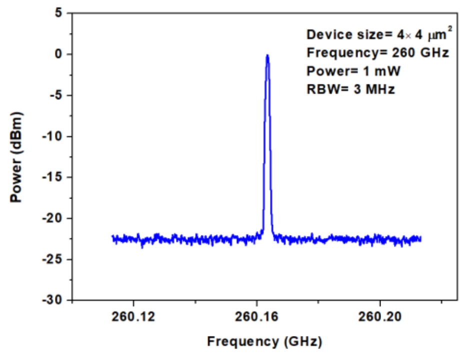

b)

Figure 9: Measured spectrum. a) 0.31 mW, 308 GHz CPW RTD oscillator, b) 1mW, 260 GHz microstrip single RTD oscillator.

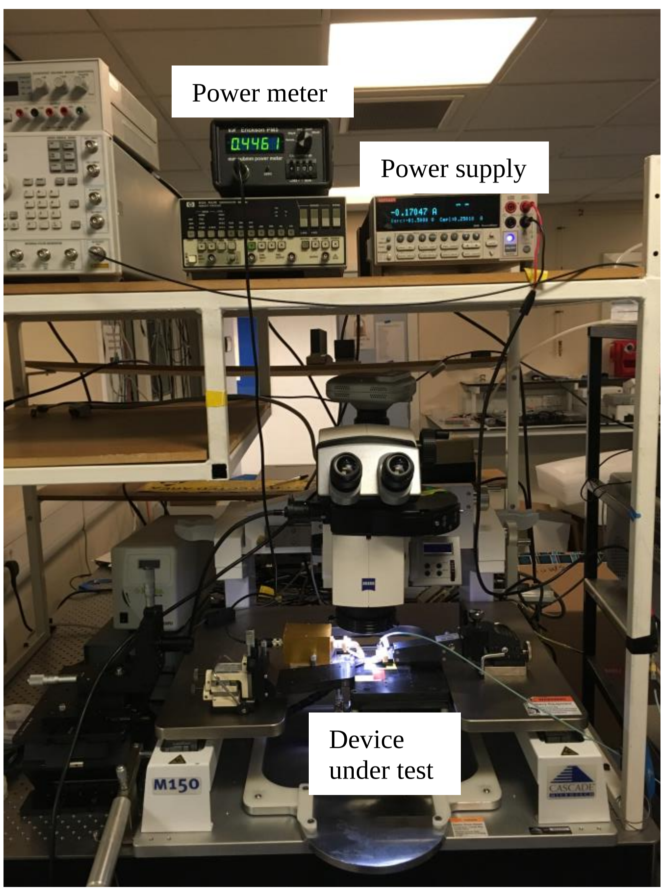

Figure 10: Actual power measurement setup of J-band oscillators. Picture of highest recorded output power from the 260 GHz microstrip RTD oscillator.

TABLE I: MEASURED (& DESIGN*) FREQUENCY, OUTPUT POWER AND DC-RF CONVERSION EFFICIENCY FOR FABRICATED RTD OSCILLATORS

Oscillator details	Osc. freq. (GHz)	Output power (mW)	dc-RF Conversion efficiency (%)
3 μm long 50 Ω CPW, Two 4 μm × 4 μm RTDs	304 (413)*	0.33	0.13
10 μm long 25 Ω CPW, Two 4 μm × 4 μm RTDs	308 (319)	0.31	0.12
7 μm long 25 Ω CPW, Two 4 μm × 4 μm RTDs	309 (356)	0.26	0.1
7 μm long 50 Ω CPW, Two 4 μm × 4 μm RTDs	245 (272)	0.42	0.17
88 μm long 10.4 Ω Microstrip, Single 5 μm × 5 μm RTD	261 (275)	0.2	0.12
88 μm long 10.4 Ω Microstrip, Single 4 μm × 4 μm RTD	260 (280)	1	0.7

V. CONCLUSION

An RTD oscillator design methodology to provide high power and high oscillation frequency at J-band was described in this paper. All the circuit components including the RTD devices are large (the smallest dimension is several microns) and so can be fabricated using photolithography. RTD oscillators offer a competitive advantage in terms of circuit simplicity and manufacturing requirements, and high output power over competing technologies. In particular, the demonstration of a single RTD device oscillator in the J-band with high output power of 1 mW shows the potential of the technology to realise compact, low-cost and high performance THz sources. The results also highlight the need for compact modelling to support the optimal design of RTD based THz sources. The proposed technology is expected to support wireless data rates of over 10 Gbps with a range of tens of meters.

REFERENCES:

[1] T. Nagatsuma, G. Ducournau, and C. C. Renaud, "Advances in terahertz communications accelerated by photonics," *Nat. Photonics*, vol. 10, no. 6 pp. 371-379, May 2016.

[2] T. Miyamoto1, A. Yamaguchi, and T. Mukai, "Terahertz imaging system with resonant tunneling diodes," *Jpn. J. Appl. Phys.*, 55, 032201 (2016).

[3] I. Kalfass *et al.*, and T. Kuerner, "Towards MMIC-based 300 GHz indoor wireless communication systems," *IEICE Trans. Electron.*, vol. E98.C, no. 12, pp. 1081-1090, Dec. 2015.

[4] M. Fujishima, S. Amakawa, K. Takano, K. Katayama, and T. Yoshida, "Terahertz CMOS design for low-power and high-speed wireless communication," *IEICE Trans. Electron.*, vol. E98.C, no. 12, pp. 1091-1104, Dec. 2015.

[5] R. Izumi, S. Suzuki and M. Asada, "1.98 THz Resonant-tunneling-diode oscillator with reduced conduction loss by thick antenna electrode," *42nd*

Int. Conf. on Infrared, Millimeter, and Terahertz Waves (IRMMW-THz), 2017, pp. 1-2.
[6] S. Diebold *et al.*, “High-speed error-free wireless data transmission using a terahertz resonant tunnelling diode transmitter and receiver,” *Electron. Lett.*, vol. 52, no. 24, pp.1999-2001, 2016.
[7] J. Wang, A. Al-Khalidi, L. Wang, R. Morariu, A. Ofiare and E. Wasige, “15 Gbps 50 cm Wireless link using a high power compact III-V 84 GHz transmitter,” *IEEE Trans. Microw. Theory Techn.*, vol. 66, no. 11, 2018, pp. 4698- 4705.
[8] J. Wang *et al*., “High performance resonant tunneling diode oscillators for THz applications,” IEEE Compound Semiconductor Integrated Circuit Symposium (CSICS), pp.1-4, 2015.
[9] J. Wang, A. Al-Khalidi, K. Alharbi, A. Ofiare, H. Zhou, and E. Wasige, “High performance resonant tunneling diode oscillators as terahertz sources,” *European Microwave Conference*, pp. 341–344, 2016.
[10] A. Al-Khalidi, J. Wang and E. Wasige, “Compact J-band oscillators with 1 mW RF output power and over 110 GHz modulation bandwidth,” 43rd *Int. Conf. on Infrared, Millimeter, and Terahertz Waves (IRMMW-THz*), 2018.
[11] A. Al-Khalidi, K. Alharbi, J. Wang, and E. Wasige, “THz Electronics for data centre wireless links - the TERAPOD project,” *9th Int. Congr. Ultra Mod. Telecommun. Control Syst.*, pp. 445–448, 2017.
[12] A. C. Cornescu et al., and E. Wasige, “High efficiency bias stabilisation for resonant tunneling diode oscillators,” *IEEE Trans. Microw. Theory Techn*., vol. 67, no. 8, pp. 3449 – 3454, 2019.
[13] R. Han and E. Afshari, “A CMOS high-power broadband 260-GHz radiator array for spectroscopy,” *IEEE J. Solid-State Circuits*, vol. 48, no. 12, pp. 3090-3104, 2013.
[14] A. Fox *et al.*, "Advanced heterojunction bipolar transistor for half-THz SiGe BiCMOS technology," *IEEE Electron Device Lett.*, vol. 36, no. 7, pp. 642-644, 2015.
[15] C. Kidner, I. Mehdi, J.R. East and G.I. Haddad, “Power and stability limitations of resonant tunneling diodes, *IEEE Trans. Microw. Theory Techn.*, vol. 38, no. 7, pp. 864 – 872,1990.
[16] C. S. Kim and A. Brändli, “High-frequency high-power operation of tunnel diodes,” *IRE Trans. Circuit Theory*, vol. 8, no. 4, pp. 416–425, Dec. 1961.
[17] K. J. P. Jacobs, B. J. Stevens, O. Wada, T. Mukai, D. Ohnishi, and R. A. Hogg, “A Dual-pass high current density resonant tunneling diode for terahertz wave applications,” *IEEE Electron Device Lett.*, vol. 36, no. 12, pp. 1295 – 1298, 2015.
[18] S. Suzuki, M. Asada, A. Teranishi, H. Sugiyama and H. Yokoyama, “Fundamental oscillation of resonant tunneling diodes above 1 THz at room temperature,” *Appl. Phys. Lett.* 97, 242102 (2010).
[19] L. Wang, “Reliable design of tunnel diode and resonant tunnelling diode based microwave and millimeterwave sources," Ph.D. Thesis, University of Glasgow, 2010.
[20] Q. Liu, A. Seabaugh, P. Chahal, and F. J. Morris, “Unified AC model for the resonant tunneling diode,” *IEEE Trans. Electron Devices*, vol. 51, no. 5, pp. 653–657, 2004.
[21] H.-J. Song and T. Nagatsuma, *Handbook of Terahertz Technologies: Devices and Applications*. Boca Raton, FL, USA: CRC Press, 2015.
[22] M. Reddy, “Schottky-collector resonant tunnel diodes for sub-millimeter-wave applications,” PhD Thesis, University of California Santa Barbara, 1997.
[23] K. Alharbi, “High performance terahertz resonant tunnelling diode sources and broadband antenna for air-side radiation,” PhD Thesis, University of Glasgow, 2016.
[24] U. Singisetti; A. M. Crook; E. Lind; J. D. Zimmerman; M. A. Wistey; A. C. Gossard; M. J. W. Rodwell, “Ultra-low resistance Ohmic contacts to InGaAs/InP,” *65th Annual Device Research Conference*, 2007
[25] http://www.keysight.com/en/pc-1297113/advanced-design-system-ads?cc=US&lc=eng

Abdullah Al-Khalidi received the BEng, MSc and PhD degrees from the University of Glasgow in 2010, 2011 and 2015, respectively. He is currently a Lecturer at the University of Glasgow. From 2015-2019, he was a postdoctoral researcher at the University of Glasgow. His main research interests include THz resonant tunnelling diodes (RTDs) and gallium nitride (GaN) transistor technologies.

Khalid Alharbi received the Ph.D. degree in Electrical Engineering from the University of Glasgow in 2016. He is currently an Assistant Professor in the Department of Electrical and Computer Engineering at King Abdulaziz University. His research interest include micro/nano-fabrication technologies, millimeter wave and THz antennas, and RTD-based devices.

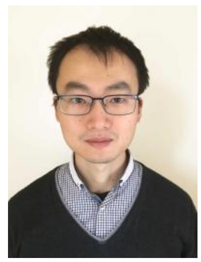

Jue Wang received the PhD degree in Electronics and Electrical Engineering from the University of Glasgow in 2014. From 2014 until now, he has been working on resonant tunneling diode based terahertz oscillator design as a postdoctoral researcher. His current research interests include high power terahertz devices and terahertz applications including wireless communications, imaging, etc.

Liquan Wang (S’11–M’12) received the B.Eng. degree in Telecommunication Engineering in 2004 from Hangzhou Dianzi University, Hangzhou, China, and the M.Sc. degree and the Ph.D. degree in Electronics and Electrical engineering from the University of Glasgow, Glasgow, U.K., in 2006 and 2012, respectively.

Since 2012, he has been with Shanghai Electro-mechanical Engineering Institute, Shanghai, China. His research interests include reliable design of high-power resonant-tunneling-diode (RTD)-based microwave and THz oscillators, RTD-driven laser diode circuits and associated applications, and the development of THz imaging systems.

Razvan Morariu received the M.Eng. degree in Electronics and Electrical Engineering in 2016 from the University of Glasgow, Glasgow, U.K., where he is currently working towards the Ph.D. degree in the design and characterization of resonant tunneling diode (RTD)-based terahertz oscillators and detectors.

Ata Khalid is a Lecturer in Sensors and Sensor Systems at Cranfield Defence and Security, Defence Academy of UK, Cranfield University, Shrivenham. He is also a visiting researcher at Glasgow University. He is an expert on compound semiconductor devices and nanofabrication technologies. His research highlights include the demonstration of the first planar InGaAs Gunn diode operation above 100 GHz leading to first terahertz planar Gunn diode operating above 300

GHz. His other research interests include mid-infrared sources and detectors based on InSb semiconductor material.

José M. L. Figueiredo (M'09) received the B.Sc. degree in Physics and the M.Sc. degree in Ooptoelectronics and Lasers from the University of Porto, Portugal, in 1991 and 1995, respectively, and the Ph.D. degree in Physics from the University of Porto in "co-tutela" with the University of Glasgow, Glasgow, U.K., in 2000. He worked with the University of Glasgow on the optoelectronic properties of resonant tunneling diodes. He is with the Department of Physics, Faculty of Sciences of the University of Lisbon. His current research interests include applications of resonant tunneling diodes and resonant tunneling diode based optoelectronic devices, and neural-inspired photonic circuits

Edward Wasige received the BSc. (Eng.) degree in Electrical Enigineering from the University of Nairobi, Kenya, in 1988, the MSc.(Eng.) from the University of Liverpool (UK) in 1990, and the PhD degree in Electrical Engineering from Kassel University (Germany) in 1999. Prior to becoming a Lecturer at the University of Glasgow in 2002, he was a UNESCO postdoctoral fellow at the Technion – Israel Institute of Technology. His current research interests include compound semiconductor micro/nanoelectronics and applications with focus on GaN electronics and RTD-based terahertz electronics.